Disponible en **www.hormigonyacero.com**
0439-5689 / Hormigón y Acero 2021; 72(294/295):59-75
https://doi.org/10.33586/hya.2021.3043

Assessment of the Efficiency of Strengthening Solutions in Concrete Structures by Means of Non-linear Step by Step Analysis Models

Evaluación de la eficiencia de soluciones de refuerzo en estructuras de hormigón mediante análisis no lineal evolutivo

Antonio Marí Bernat[a], Jesús M. Bairán García[a] y Eva Oller Ibars[a]

[a] *Department of Civil and Environmental Engineering. Universitat Politècnica de Catalunya*

Recibido el 30 de noviembre de 2020; aceptado el 12 de febrero de 2021

ABSTRACT

When designing a structural strengthening solution, the influence of the previous state of the structure on the capacity of the strengthened structure must be evaluated. In addition, strengthening interventions may involve operations such as partial unloading of the structure, placement and removal of temporary shores, application of loads or pre-deformations, restoring of damaged reinforcement or spalled concrete or constraining of lateral strains. Therefore, changes in the cross-section geometry and reinforcement, longitudinal scheme, support conditions, loads and state of stresses and strains, may take place. Furthermore, occurrence of phenomena producing a premature failure or a change in the failure mode, should be avoided. In order to account for such a large variety of causes and phenomena affecting the structural response, a nonlinear and time-dependent analysis model of 3D reinforced and prestressed concrete frames, capable of capturing different failure modes and taking into account the structural history, is described. The model has been verified with tests on strengthened structures available in the literature and has been applied to an actually remodeled structure, comparing the advantages and disadvantages of two different strengthening proposals, showing its capabilities to assess the efficiency of structural strengthening systems..

KEYWORDS: Strengthening, remodelling, non-linear analysis, assessment, reinforced concrete, prestressed concrete.

RESUMEN

Al diseñar una solución de refuerzo estructural, se debe evaluar la influencia del estado tenso-deformacional previo de la estructura en la capacidad portante de la misma después del refuerzo. Además, las intervenciones de refuerzo pueden involucrar operaciones tales como la descarga parcial de la estructura, colocación y retirada de puntales provisionales, aplicación de cargas o pre-deformaciones, restauración de armaduras dañadas o hormigón desconchado o constreñimiento de deformaciones laterales. Por tanto, pueden producirse cambios en la geometría de la sección transversal y en la armadura, en el esquema longitudinal, en las condiciones de apoyo, en las cargas y en el estado tensodeformacional. Además, debe evitarse la aparición de fenómenos que produzcan el fallo prematuro o un cambio en el modo de rotura. Para tener en cuenta la gran variedad de causas y fenómenos que afectan la respuesta estructural, en este artículo se describe un modelo de análisis no lineal evolutivo en el tiempo de pórticos tridimensionales de hormigón armado y pretensado, capaz de captar diferentes modos de rotura y teniendo en cuenta la historia de la estructura. El modelo ha sido verificado reproduciendo ensayos sobre estructuras reforzadas disponibles en la literatura y ha sido aplicado a una estructura real remodelada, comparando las ventajas y desventajas de dos propuestas de refuerzo diferentes, mostrando su capacidad para evaluar la eficiencia de los sistemas de refuerzo estructural.

PALABRAS CLAVE: Refuerzo, remodelación, análisis no-lineal, evaluación, hormigón armado, hormigón pretensado.

* Persona de contacto / *Corresponding author*:
Correo-e / *email*: eva.oller@upc.edu (Eva Oller Ibars).

Cómo citar este artículo: Marí Bernat, A., Bairán García, J.M., Oller Ibars, E. (2021) Assessment of the Efficiency of Strengthening Solutions in Concrete Structures by Means of Non-linear Step by Step Analysis Models, *Hormigón y Acero*, 72(294-295), 59-75, https://doi.org/10.33586/hya.2021.3043

1. INTRODUCTION

Strengthening of structures may be necessary, among other reasons to: 1) restore the load carrying capacity and functionality of structures deteriorated or damaged by environmental or mechanical actions; 2) resist increments of loads due to changes in the use of the structure or in the nominal loads established by the design codes; 3) seismic retrofit or adaption of the structure to resist extraordinary actions; 4) allow the remodelling or enlargement of structures; and 5) modify the dynamic response, avoid inadmissible vibrations or resonance [1–5].

Faced with one of these situations, there is a number of actions to be carried out. These actions are: 1) identify the problem and characterize the state of the structure; 2) define the objectives of the intervention; 3) propose alternative solutions; 4) evaluate the resistant capacity of the original structure; and 5) evaluate the capacity of the strengthened structure in order to assess the efficiency of the intervention.

Among the many types of interventions, those that can be considered the most common are [6–9]:

- Enlargement of cross section with concrete or special mortars and reinforcements, properly connected to the original section.
- Placement of steel plates or fiber-reinforced polymers (FRP) laminates bonded with epoxy resin or mechanically anchored to the element.
- External prestressing, introducing a desired load system to balance exterior loads, compress the concrete or connect an enlargement to the original element.
- Passive or active confinement, placing steel shapes or plates, enlarging the section with reinforced concrete or wrapping with FRP or with prestressing wires or strands.
- Provision of additional support structures to reduce spans or the load supported by each element.

These strengthening interventions use to require carrying out actions such as: total or partial unloading of the structure, placement of temporary shores, application of loads or pre-deformations, cleaning of the deteriorated zones, injection of cracks, bond surface preparation, restoring of reinforcement or spalled concrete, among others. Such actions may considerably affect the structural response during and after strengthening. In fact, changes in the cross-section, in the longitudinal scheme, in the support system, in the amounts of reinforcement, in the state of loads, stresses and deformations, may take place.

In addition, the design of a strengthening solution must comply with a series of basic principles, in order to achieve the planned objectives [10–11]. The following aspects affecting the adequacy and efficiency of the strengthening must be considered, among other issues:

- Occurrence of phenomena that may prevent arriving to the target ultimate load or producing a premature failure should be avoided. Examples are the debonding of an externally bonded steel plate or FRP sheet, changes in the failure mode (from ductile to brittle or from flexure to shear) or failure of elements different from that being strengthened.
- The effects of the construction process and load history of the original structure on its stiffness, state of stresses and strains and resistance should be assessed.
- The effects of previous damage of the original structures on the capacity of the strengthened structure should be investigated. For instance, how previous cracking or reinforcement corrosion may affect the flexural strength of a strengthened column.
- The influence of the strengthening operation procedure adopted, and of the existing loads acting on the original structure during the strengthening operations, should be taken into account. In fact, as a matter of example, unloading the structure allows the strengthening system to be more efficient, since then, it is effective even for the permanent loads.

From the above considerations, it can be concluded that a sound assessment of the structural efficiency of the strengthening system is not straightforward, since some aspects related to the load history, previous damage and failure modes must be adequately taken into account. For this purpose, load tests, theoretical considerations and structural analyses are considered adequate tools. However, due to the complex phenomena involved and the cost of experimental analyses, structural analyses based on numerical models have become a very powerful tool when assessing the performance of existing structures, either affected by previous damage, by remodeling or by strengthening interventions.

Among the large variety of numerical structural models currently available for frame structures, very few of them [12] take into account the effects of load history, construction procedure or previous damage in the original structure on the performance and strength of the strengthened structure. In order to account for such capabilities, step-by-step or phased analysis is required. Furthermore, most of the models capable to capture the complexity of the phenomena involved are based on 2D or 3D Finite Elements simulations, which are very costly and time consuming, so their use can be justified when analysing local effects rather than the global structural performance.

In this paper, a numerical model for the global nonlinear step-by-step analysis of three dimensional reinforced and prestressed concrete frames, capable to account for most events that may occur and affect the structure response along its service life, is described. The model was initially developed to capture the flexural behaviour of simultaneously constructed 3D frames [13] and it was subsequently completed to account for segmental construction [14], for deterioration, strengthening and remodelling [15]. More recently a relevant improvement was done by including the effect of combined shear and normal stresses in the structural response and strength [16], providing the model with the capacity to predict the shear-flexure interaction, shear failures and the effects of shear strengthening [17–20] with different strengthening techniques.

2. DESCRIPTION OF THE ANALYTICAL MODEL

2.1. Flexural model

2.1.1. Structure idealization and nonlinear time-dependent strategy

A filament beam element (figure 1) with arbitrary cross-section and 13 degrees of freedom is used by the model. The cross-section

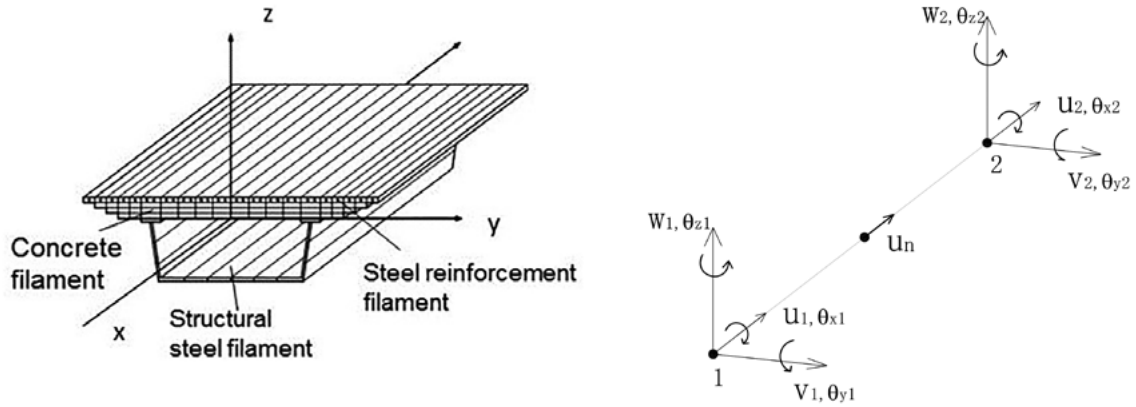

Figure 1. Filamented beam element: Section idealization and degrees of freedom.

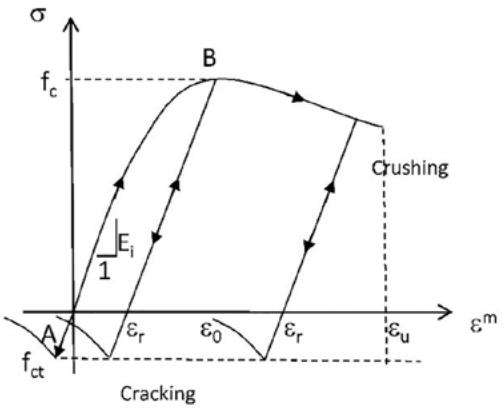

Figure 2. Concrete σ - ε relationship.

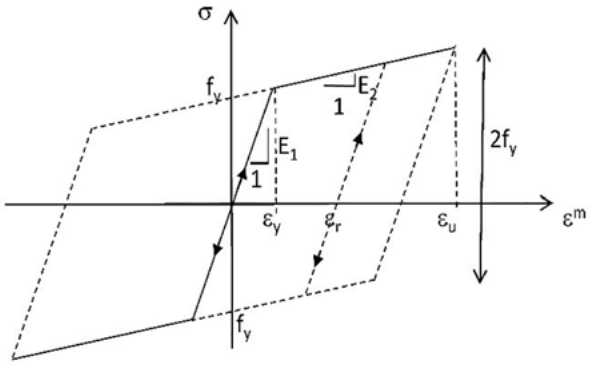

Figure 3. Reinforcing steel σ - ε relationship.

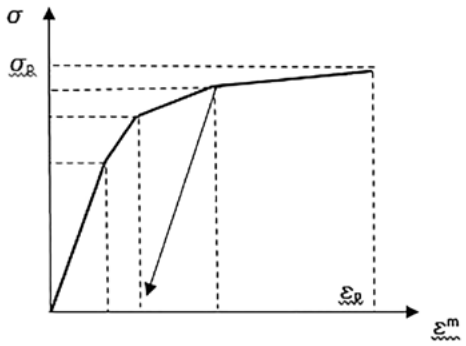

Figure 4. Prestressing steel σ - ε relationship.

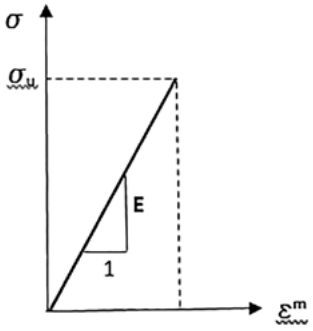

Figure 5. FRP σ - ε relationship.

is divided into filaments of concrete, reinforcing steel or structural steel. Each filament is subjected to a uniaxial stress state, so shear strains are neglected, and the hypothesis of plane sections deformation is adopted. The model can take into account the material and geometrical non-linearities as well as the time effects due to creep, shrinkage and relaxation of prestressing steel.

Non-linear constitutive equations for the concrete (figure 2), reinforcing (figure 3) and prestressing steel (figure 4) are used to account for the non-linear response under increasing loading levels, including load reversals.

When using fibre reinforced polymers as strengthening materials, a linear-brittle stress-strain relationship is adopted (figure 5).

The total strain at a given time and point in the structure $\varepsilon(t)$, is taken as the direct sum of mechanical strain $\varepsilon_m(t)$ and non-mechanical strain $\varepsilon_{nm}(t)$. Mechanical strain is the instantaneous strain caused by short-time loading and is the independent variable in the stress-strain relationship. Non-mechanical strain consists of creep strain $\varepsilon_{cr}(t)$, shrinkage strain $\varepsilon_{sh}(t)$, aging strain $\varepsilon_a(t)$, and thermal strain $\varepsilon_T(t)$.

Creep strain $\varepsilon_{cr}(t)$ of concrete is evaluated by an age dependent integral formulation based on the principle of superposition. Thus,

$$\varepsilon_{cr}(t) = \int_0^t c(\tau, t-\tau)\, \frac{\partial \sigma(\tau)}{\partial \tau}\, d\tau \qquad (1)$$

where $c(t, t\text{-}\tau)$ is the specific creep function, dependent on the age at loading τ, and $\sigma(\tau)$ is the stress applied at instant τ. Numerical creep analysis may be performed by subdividing the total time interval of interest into time intervals Δt, separated by time steps. The integral (1) can then be approximated by a finite sum involving incremental stress change over the time steps. The adopted form for the specific creep function $c(t, t\text{-}\tau)$ is a Dirichlet series:

$$c(\tau, t-\tau) = \sum_{1}^{m} a_i(\tau)[1 - e^{-\lambda(t-\tau)}]d\tau \quad (2)$$

where m, λ_i, and $a_i(t)$ are coefficients to be determined through adjustment of experimental or empirical creep formulae, as recommended by international codes, by least squares fit. In this work, it is considered that sufficient accuracy is obtained using three terms of the series ($m = 3$), and adopting $\lambda_i = 10^{-i}$. The use of a Dirichlet series allows obtaining the creep strain increment at a given instant by a recurrent expression that only requires to store the stress and an internal variable of the last time step, thus avoiding the need to store the entire stress history when analysing large structures.

Shrinkage strain at any time can be obtained from code provisions or from specific tests. A detailed explanation of ageing and temperature strains can be found in Marí [13]. A logarithmic curve is used as pre-stress relaxation function, assuming a constant strain. However, a fictitious initial stress, is used to account for the reduction of stress in the tendons due to other actions (creep, shrinkage or external loads).

In this study, for the time dependent analysis, the time domain is divided into a discrete number of time intervals, and the junctions of these intervals are called time steps. A step forward integration is performed by adding the results obtained for each time step successively, starting from the first-time step to arrive to the final solution. At any time step the increment of total strain at any point, resulting from the structural analysis, is accumulated over the previous one. Then, the mechanical strains are obtained by subtracting from the total strains the accumulated non-mechanical strains. Then, the stresses are computed from the non-linear constitutive equations, as a function of the accumulated mechanical strains.

Iterative procedures combined with incremental analyses are used to trace the structural response throughout the elastic, cracked and ultimate load levels. Load control and displacement control strategies (for structures that exhibit strain softening or snap-through) are used together with Newton-Raphson algorithms, in which the stiffness matrix and the amount of unbalanced forces introduced at each iteration are in accordance with the level of cracking and damage of the structure. At each time step, the structure is analyzed under the external applied loads and under the imposed deformations, such as creep, shrinkage and thermal strains, originated during the previous time interval and geometry.

$$\Delta R = \Delta R^{i} + \Delta R^{nm} + \Delta R^{u} = K\delta \quad (3)$$

where the total load vector ΔR is composed by the vectors due to the internal stresses (ΔR^{i}), non-mechanical strains, (ΔR^{nm}) and unbalanced forces due to non-linearities (ΔR^{u}) of the previous iteration, K is the updated stiffness matrix according to the materials state and δ is the vector of nodal displacements. Nodal displacements, element internal forces, stresses and strains in each concrete and steel filament, curvature and elongation of each section, support reactions and other response parameters are provided by the model, after convergence is reached.

Pre-tensioned and post-tensioned structures with straight or parabolic tendons can be analysed. When stressing, the equivalent prestressing forces obtained by equilibrium of the tendons are applied over the structure. Variations of stresses and tendons force are obtained for each load step by considering strain compatibility between the concrete and the pretressing segments and subtracting the relaxation of stresses along the elapsed time. The prestressing loads are, then, updated and the new system of non-linear equations is set.

Most modifications that may take place during the construction process and along the service life, such as deterioration of materials areas and properties, changes in the longitudinal and cross sections geometry, structural scheme, material properties and applied loads, can be simulated by the model, through a step-by-step solution scheme, as explained next. The described numerical model has been implemented in a computer program called CONS.

2.1.2. Simulation of the structural effects of reinforcement corrosion

The above-described model was modified to reproduce the effects of corrosion due to carbonation, that produces a loss of steel area, more or less uniformly distributed around the reinforcing bars. A law defining the reduction of steel area was adopted, which depends on the rate of corrosion, given in µmm/year of reduction of the bar diameter. The evolution of the bar diameter is considered proportional to the corrosion velocity [21].

The loss of steel area results in a reduction in capacity and in stiffness of any cross section affected by corrosion. Thus, when performing the computation of internal forces, by integration of the stresses, the external forces will not be balanced by the internal ones. Then, these unbalanced forces are automatically introduced in the non-linear iterative scheme, until equilibrium is obtained. As a consequence of corrosion, increments of stresses and strains in concrete and steel, increments of deflections (due to the loss of stiffness) and redistribution of internal forces takes place to satisfy equilibrium and compatibility conditions for the current state of the materials.

2.1.3. Simulation of the structural effects of strengthening

The element cross-section can be formed by parts constructed in different instants and composed by different materials. For each concrete, reinforcing steel or element, the instant of placement and the instant of removal are defined. Furthermore, at each construction step, changes in the element's connectivity, in the support conditions, introduction of prestressing force or imposed deformations, and application of loads and imposed displacements are defined.

In this way, adding or removal of concrete parts, reinforcing bars, prestressing tendons or elements can be simulated. Consequently, the following situations related to remodelling and strengthening of structures are taken into account: spalling of concrete cover, substitution of damaged concrete parts or reinforcing bars, enlargement of concrete cross section, place-

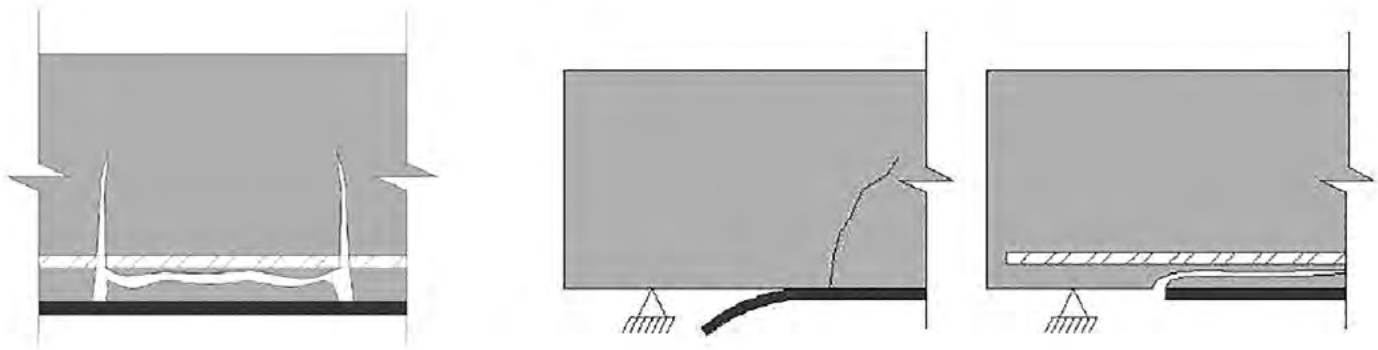

a) b.1) b.2)

Figure 8. a) Intermediate crack debonding; b.1) laminate end debonding at the interface; b.2) laminate end debonding with concrete ripping-off.

ment of new reinforcement bars, steel plates or bonded FRP laminates, placement or removal of temporary shores, imposed movements, blocking of pins, monolithically connection between elements and application of external prestressing, among others.

With this scheme, the response of structures before and after the strengthening can be obtained, including the effects of previous damage and those of the repair, retrofit or strengthening operations.

2.1.4. Adopted debonding model

According to current state-of-the-art, debonding is the most common failure in existing structures strengthened in flexure by FRP externally applied reinforcement. As described in Fib Bulletin 90 [9], debonding failure can initiate either at intermediate cracks due to shear stresses, or at the laminate end (figure 8).

The debonding failure approach implemented in the present model is that proposed by Oller et al. [22], that prevents laminate debonding at intermediate cracks and at the laminate end. To avoid debonding at intermediate cracks, the laminate tensile force increment between two cracks is limited to the maximum increase in tensile stress that can be transferred by means of bond stresses along the crack spacing ($\Delta P_{max,scr}$). In the literature, there are other similar approaches based on the envelope of tensile stresses that depend also on the crack spacing [9,23–29]. In addition, Matthys [30] developed an approach that limits the interfacial shear stress resulting from the change of tensile force along the FRP reinforcement that does not depend on the crack spacing. D'Antino and Triantafillou [31] assessed the performance of some of the existing debonding models, concluding that the model of Said and Wu [28] showed the best performance. A similar analysis was previously developed by Oller et al. [32]. According to this analysis, the simplified model of Oller et al. [32] and the models of Ye et al. [24] and Said and Wu [28] showed the best statistical performance in terms of mean value and coefficient of variation. According to Oller et al. [22], the maximum transferred force along the crack spacing $\Delta P_{max,scr}$, can be expressed as:

$$\Delta P_{max,s_{cr}} = \frac{(1-\upsilon)}{\left(1- \cos\frac{\pi L_b}{2L_{lim}}\right)} P_{max,L_b} \quad (4)$$

where υ = ratio between the lower and the higher laminate tensile stresses in both cracks, named, σ_{fI} and σ_{fJ} respectively; L_b = remaining bonded length calculated as the minimum value between the estimated crack spacing, s_{cr}, and the limit, scr,lim, between a short ($s_{cr} \leq s_{cr,lim}$) and a long crack spacing ($s_{cr} \geq s_{cr,lim}$), given by Eq. (5); L_{lim} = limit between a short and a long bonded length in an equivalent pure shear specimen given by Eq. (6); $P_{max,\ L=Lb}$ = maximum transferred force of an equivalent pure shear specimen whose length is L_b, given by Eq. (7).

$$s_{cr,lim} = 0.637 L_{lim} \arccos \upsilon \quad (5)$$

$$L_{lim} = \frac{\pi}{2}\frac{\sqrt{2G_F E_f t_f}}{\tau b_M} \quad (6)$$

$$P_{max,L_b} = P_0 \begin{cases} sin\left(\frac{\pi}{2}\frac{L_b}{L_{lim}}\right) & L_b \leq L_{lim} \\ 1 & L_b > L_{lim} \end{cases} \quad (7)$$

$$P_0 = b_L \sqrt{2G_F E_f t_f} \quad (8)$$

where: b_f, t_f = laminate width and thickness respectively; E_f = laminate modulus of elasticity; τ_{bM} = maximum shear stress given by Eq. (9); G_F = fracture energy or energy by unit area necessary to separate the laminate from the support given by Eq. (10).

$$\tau_{bM} = C_{\tau_{bM}}\left(\frac{1}{f_{ctm}} + \frac{1}{f_{cm}}\right)^{-1} \quad (9)$$

$$\tau_{bM} = C_{\tau_{bM}}^2 C_F f_{ctm} \quad (10)$$

where f_{cm} = mean value of concrete compressive strength; f_{ctm} = mean value of concrete tensile strength; $C_{\tau_{bM}}$ = constant with a mean value of 0.87 and a standard deviation of 0.17 according to the shear test database assembled by the authors; C_F = constant with a mean value of 0.35 and a standard deviation of 0.07.

To avoid laminate end debonding, the laminate tensile force increment between the laminate end and the nearest crack, should be limited to a maximum value given by $\Delta P_{max,L_b}$ that can be obtained by Eq. (7) for an element between the

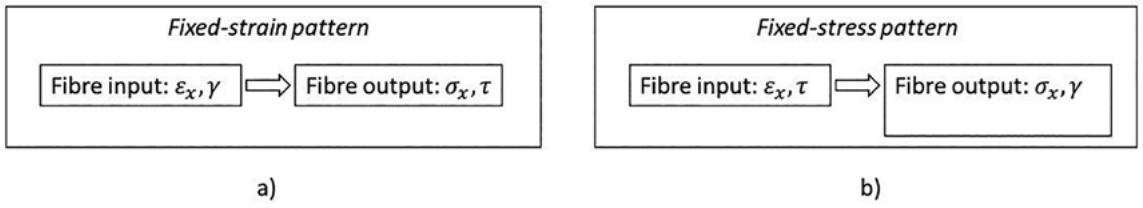

Figure 9. Two types of fixed patterns for shear analysis in frames. a) fixed-strain, b) fixed-stress.

laminate end and the nearest crack ($L_{b,end}$), by assuming $L_b = L_{b,end}$ and $\upsilon = 0$ ($\sigma_{f,I} = 0$).

This criterion can be easily implemented in the present non-linear structural analysis model, since the layered idealization of the cross-section allows determining the shear stress at any concrete, steel or FRP reinforcements, by setting the equilibrium of normal forces at the laminate in the two Gauss integration points of each element.

In order to evaluate the shear force transmitted by the laminate between two adjacent cracks, the above calculated force is multiplied by the ratio s_{cr}/d_g, being scr the crack spacing and d_g the distance between Gauss points. This criterion of proportionality requires the element length to be equal or greater than the crack spacing, what is generally acceptable.

When the force between cracks causes debonding failure, according to the above criterion, the laminate is automatically removed from the corresponding element in the model. If the structure is capable to reach equilibrium, by means of non-linear redistributions at the section and at global levels, the analysis continues; otherwise, the structure failure takes place.

2.2. Shear model

The previously described flexural model was extended to account for the effects of in-plane shear in Ferreira et al. [33,34], and the resulting model is here referred as CONSHEAR. The new model inherits the sequential construction capabilities; hence, it can be applied to problems involving sequential construction, deterioration and repair in shear sensible concrete structures, see [16,17,35]. In the following, the extensions to include shear effects in CONS model, are described.

2.2.1. Accounting for shear stresses in frame models

Shear loading always is in combination with bending moments; therefore, each material point is subjected, at least, to biaxial loading. Uniaxial stress-state is the main limitation of traditional frame formulations to effectively consider shear effects in the non-linear behaviour. Some successful formulations have been developed based on different hypotheses to allow some kind of multiaxial stress-strain distribution in the cross-section, e.g. Bairan and Marí [36,37], Ceresa et al. [38], Navarro-Gregori et al. [39], Mohr et al. [40], Le Corvec [41], di Re [42], Kagermanov and Ceresa [43], Poliotti and Bairan [44], among others.

Bairan and Marí [45] developed a detailed state-of-the-art review; identifying three main types of approaches: fixed-strain pattern, *fixed-stress pattern and explicit inter-fibre equilibrium*. The fixed-strain pattern mimics the process used in the traditional frame models by adding a pre-selected shear strain distribution to the plain-section hypothesis. This method allows a direct implementation in the classical frame formulations, as the input of the sectional analysis is the normal and shear strains and the output is the corresponding stresses and their integration, see figure 9a. However, as demonstrated in [40], it fails to capture the subsequent variations in the post-cracking and post-yielding phases, showing excessive concentration of shear stresses in the compression head of the beam and not adequate valuing the effects of transverse reinforcement.

In CONSHEAR, a fixed-stress pattern was developed. This approach allows a better prediction of the shear strain distribution after cracking and yielding. Figure 9b shows that the cross-section model is not standard: its input is the combination of normal strains and shear stresses, and the output is the normal stress, shear strain and the transversal strain that activates the transverse reinforcement after cracking, see figure 10. The biaxial stress-strain components result from an internal equilibrium of each concrete layer and the stirrups describes as follows.

As described in figure 11, the user classifies the fibres of a cross-section into normal-stress fibres (figure 11a), where the material behaviour is considered as uniaxial, and shear-resisting fibres (figure 11b), with biaxial loading.

During a particular time step, the increment of shear force is distributed on the shear-resisting fibres. Eq. (11) shows the increment of shear stress, where $A*$ is area of the active shear-resisting fibres.

$$\Delta\tau_{xy}^{c} = \frac{\Delta V}{A^{*}} \tag{11}$$

As shown in recent studies [46,47], flanges in compression may contribute significantly to the ultimate shear capacity. Therefore, the shear effective area may include some fibres of the flange. Notice, however, that both fraction of shear resisted by the flange fibres varies, in general, with the cracking stage. An analysis of these effects can be found in [48], which may also serve as basis for the selection of flange area.

Normal strains of all types of fibres are distributed after the plane-section hypotheses, see Eq. (12). The response of the normal fibres is completed defined by the acting strain and the uniaxial constitutive model of the material. However, in the case of shear-resisting fibres, the transversal response needs to be computed.

$$\varepsilon_x^c(z) = \Delta\varepsilon + \Delta\phi_y z \tag{12}$$

The transversal strain is computed by balance of forces in the transversal direction, involving the tension of transverse reinforcement and the compression the layer of fibres, figure 11b. This represents the internal condition of Eq. (13), which should be satisfied in every layer, where ρst is the transversal steel ratio ($\rho st = Astblayer\ st$).

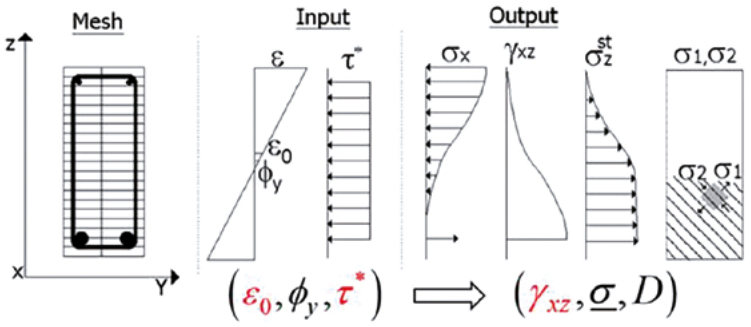

Figure 10. Hybrid sectional analysis implemented in CONSHEAR.

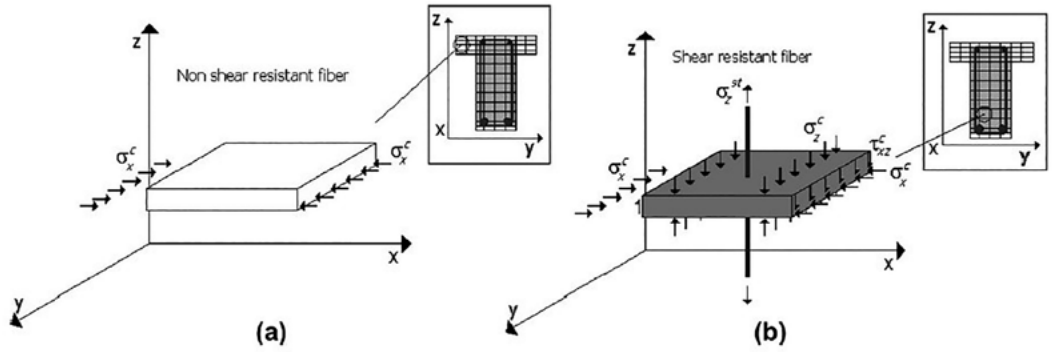

Figure 11. Types of fibres in the CONSHEAR sectional analysis. a) Normal stresses fibres, b) Shear-resisting fibres.

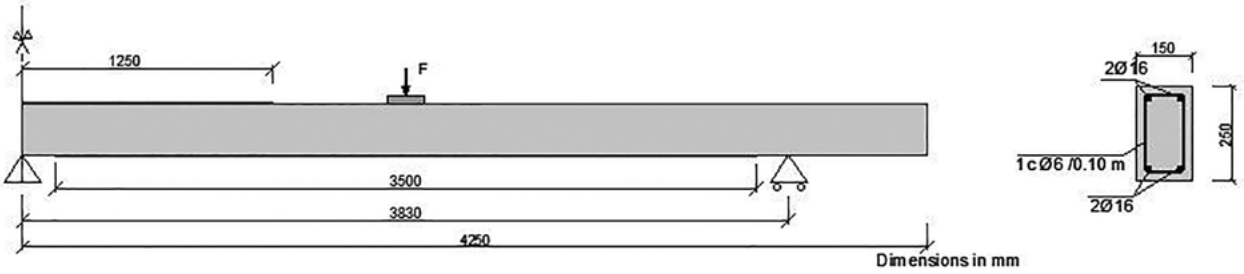

Figure 12. Geometry and test set-up of Beams E1, E2, E3 and E4.

$$\Delta\sigma_x^c + \rho_{st} z \Delta\sigma_z^{st} = 0 \qquad (13)$$

After inclined cracking, solution of Eq. (13) requires a suitable biaxial constitutive model for the concrete. For more details on the constitutive model implementation are in found in [36].

3. EXPERIMENTAL VERIFICATION OF THE MODEL

3.1. Continuous RC beam strengthened in flexure with FRP

El-Refaie et al. [49] tested five reinforced concrete continuous beams of two equal spans, strengthened in flexure with externally bonded carbon fibre reinforced polymer (CFRP) laminates, in order to study the influence of the position and form of the external reinforcement. The performance of the CFRP strengthened beams was compared with that of an unstrengthened control beam. Debonding failure was the dominant mode of failure for all the strengthened tested beams. Beams E1 (unstrengthened), E2, E3 and E4 are analysed and compared with the experimental results.

The beam geometry, the internal reinforcement, the loading and support arrangement are illustrated in figure 12. Each beam was 8500 mm long, 150 mm wide and 250 mm deep. The longitudinal reinforcement consists of four 16 mm diameter bars. The concrete cover was 32 mm, so the effective depth was 218 mm. Closed stirrups of 6 mm diameter spaced at 100 mm along each beam were provided to prevent shear failure.

CFRP laminates of 100 mm x 1.2 mm were bonded in the top face of beams E2 and E4, and on the bottom face of beams

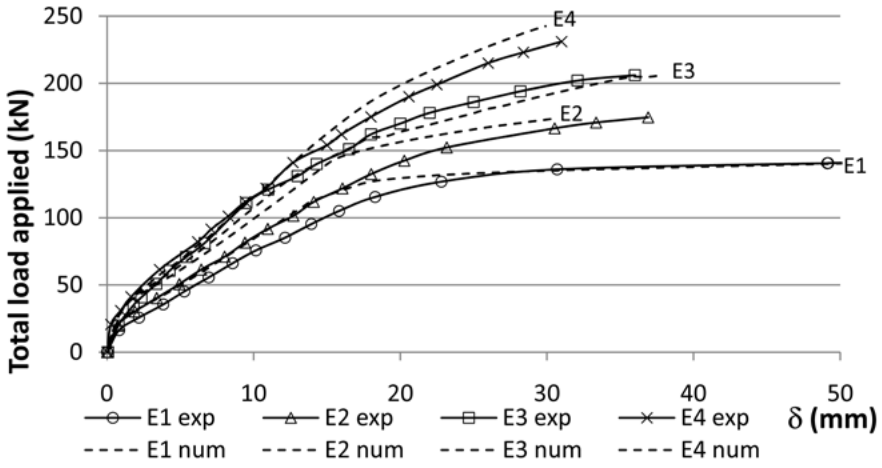

Figure 13. Experimental vs numerical applied load vs midspan displacement.

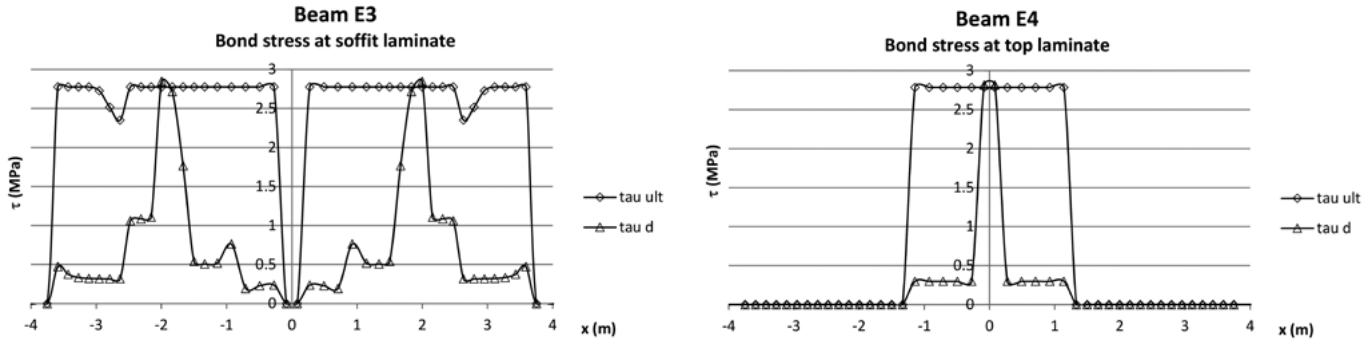

a) b)

Figure 14. Experimental vs. numerical bond stress distribution for beams: a) E3 and b) E4.

E3 and E4. The laminates applied to the top face of the beams were 2500 mm long and were placed symmetrically about the line of the central support. Those applied to the bottom face of the beam were 3500 mm long and were positioned symmetrically about the centres of both spans.

The material properties of the tested beams are those reported in [49]. For the performed analysis, the compressive cube strength and the rupture tensile strength experimentally obtained have been transformed into the cylinder compressive strength and the direct tensile strength, respectively, as summarized in table 1. The values proposed by Eurocode 2 [50] for other parameters of the concrete stress-strain relationship, such as the initial modulus of elasticity E_c, the peak and ultimate strains, have been adopted. The maximum shear stress τ_{LM} and the fracture energy G_F have been calculated according to the mean values of $C\tau_{LM}$ = 0.87 and C_F = 0.35. The crack spacing has been calculated according to the Spanish Concrete Code [51] and has resulted to be scr = 85 mm. The properties for the longitudinal reinforcement steel are: yielding strength f_{sy} = 520 N/mm^2; ultimate strength f_{su} = 630 N/mm^2; and modulus of elasticity E_s= 200000 N/mm^2. The nominal ultimate strength of the CFRP laminates is f_{fu} = 2500 N/mm^2 and their modulus of elasticity is E_f = 150000 N/mm^2.

A total of 25 beam elements of equal length (226 mm) was used in the analysis. The cross section was divided into 50 layers each of 5 mm depth.

TABLE 1.
Concrete properties used in the analysis. Units are N and mm.

Beam	E1	E2	E3	E4
Compression cube strength f_{cu}	24.0	43.6	47.8	46.1
Compression cylinder strength estimated	21.6	39.2	43.0	41.5
Modulus of rupture f_r	3.00	4.60	4.40	4.40
Direct tensile strength f_{ct} estimated	2.22	3.41	3.25	3.25
Max. shear stress for peeling failure τ_{LM}	--	2.77	2.88	2.89
Fracture Energy G_F (N mm/mm^2)	--	1.19	1.14	1.14

Figure 13 shows the experimental and the theoretical load-displacement relationships for the four beams analysed. Excellent agreement is obtained in the ultimate capacity, the displacements, and the shape of all the compared curves. The only remarkable difference is in the ultimate displacement of beam E2, for which the theoretical model predicts FRP debonding failure for a displacement of 31 mm in spite of 39 mm measured experimentally. In all cases,

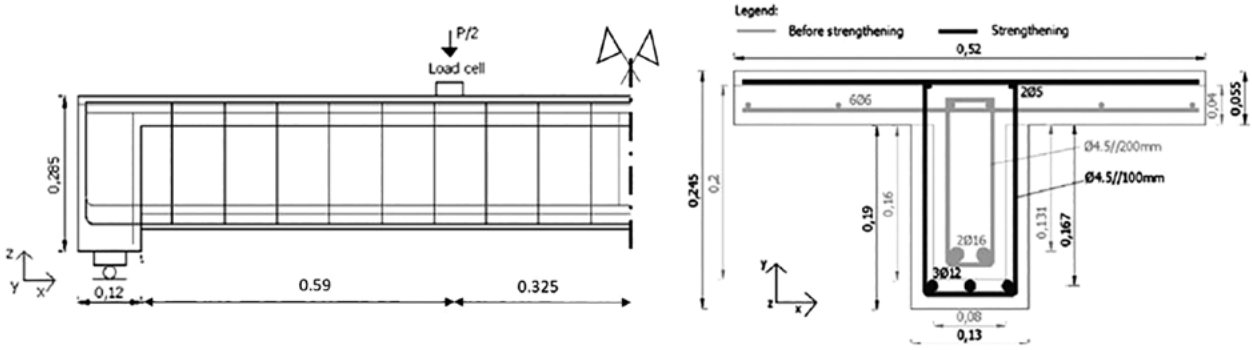

Figure 15. Test set-up, geometry and reinforcement of the beam before and after strengthening (adapted from [53]).

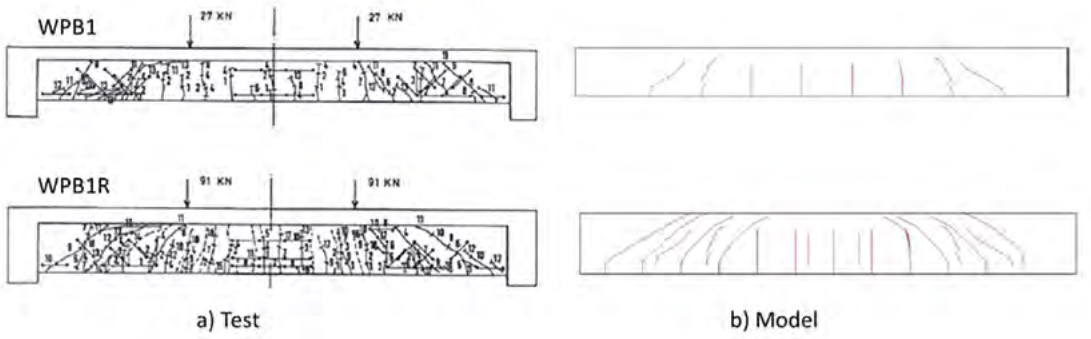

Figure 16. Crack pattern under first damage (WPB1) and repaired structure at failure (WPB1R). a) Experimental observation, b) Model prediction.

the model correctly predicted the ultimate load as well as the type of failure.

Figure 14a and 14b show the bond stress distribution (τ_d) and the calculated bond strength (τ_{ult}) along the beam length for beams E3 and E4, respectively. A premature debonding failure occurs once the bond stress (τ_d) reaches the bond strength (τ_{ult}) at a certain point of the interface. It can be observed that debonding failure takes place at beam E3 at the soffit laminate under the applied point load, for a bond stress of 2.77 N/mm^2 and at beam E4 over the central support, for a bond stress of 2.78 N/mm^2.

From the comparison between the experimental and the theoretically obtained results, it can be concluded that the model is capable to capture the structural response not only in the load-deflection curves but also in the internal forces, reactions, stresses, strains, ultimate load and failure mode, including debonding failures. More details about this modelization can be found in [52].

3.2. *Shear strengthened reinforced concrete beam*

The shear tests carried out by Souza and Appleton [53] are simulated in the following. This analysis investigates the specimen that was loaded to produce shear damage and further repaired with additional transversal reinforcement and shotcrete enlargement. In the original publication, this sequence is referred as test WBP1, for the first loading producing shear damage, without collapse, and WBP1R for the second test on the repaired structure.

Figure 15 describes the geometry and reinforcement of the original and repaired specimens. The mechanical properties of the concrete and the time of test are defined in table 2. Similarly, table 3 describes the mechanical properties of the reinforcement.

The first load on the original specimen (WBP1) was P=54 kN. The specimen was then unloaded and repaired. Subsequently, the element was tested until failure (WBP1R), with a load P=182 kN. Figure 16a shows the crack pattern of the first and failure tests.

TABLE 2.
Concrete mechanical properties.

	Properties at 28 days			
Specimen WPB1R	f_c (MPa)	f_{ct} (MPa)	E_c (GPa)	Day of test
Damaged	32	3.3	29	102
Strengthened				226
Shotcrete	36	4.5	23	103 (repairing)

TABLE 3.
Reinforcement mechanical properties

Diameter (mm)	f_y (MPa)	f_{su} (MPa)	E_s (GPa)
4.5	490	532	193
6	488	706	180
12	401	636	196
16	448	674	201

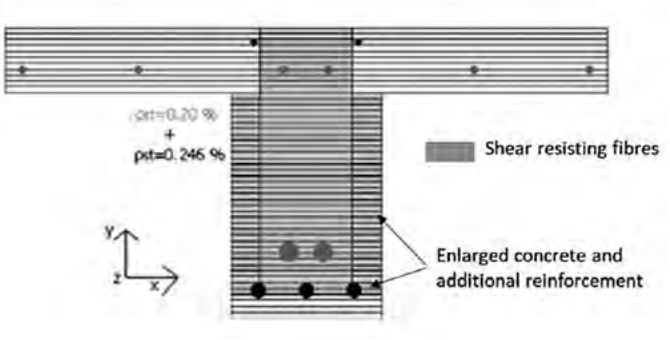

Figure 17. Modelled cross-section layers, showing the fibres of the original specimen and the shotcrete enlargement (based on [17]).

The structure was modelled using CONSHEAR with 30 Timoshenko elements with linear interpolation. Figure 17 shows the cross-section discretization, where the fibres of the original concrete and the shotcrete enlargement can be observed. In this analysis, the shear resisting fibres consists of the fibres of the original web and the concrete enlargement. The longitudinal reinforcement are presented in the corresponding location. The transverse reinforcement was modelled through steel ratios of 0.2% in the original element and an additional ratio of 0.246% after repairing.

Figure 16b shows the predicted crack patterns for first loading (PB1) and in the repaired case (WPB1R) at failure. As observed, the overall damage pattern and crack inclinations are well captured.

Figure 18 shows the comparison of the experimental tests with the numerical prediction using the model CONSHEAR and the response of the original CONS model that does not include shear interaction effect. Figure 18 compares the load deflection in the two stages. Both in the first loading and the loading up-to-failure of the repaired structure, the model without shear effects predicts significantly larger stiffness than the observed in the test. Conversely, the model CONSHEAR correctly captures the element stiffness. Moreover, CONS predicts a ductile response (figure 19b), while the CONSHEAR can capture the early shear failure.

Figures 18c to 18f show the local reinforcement strains in the section located at 0.36 m from the support. The strains in the longitudinal reinforcement are described in Figs. 18c and 18d. The shear-bending interaction produces additional strains (and stresses) than the produced solely by the bending moment. The model CONS does not capture this effect, while CONSHEAR correctly capture the trends of the force-strain evolution, particularly after cracking.

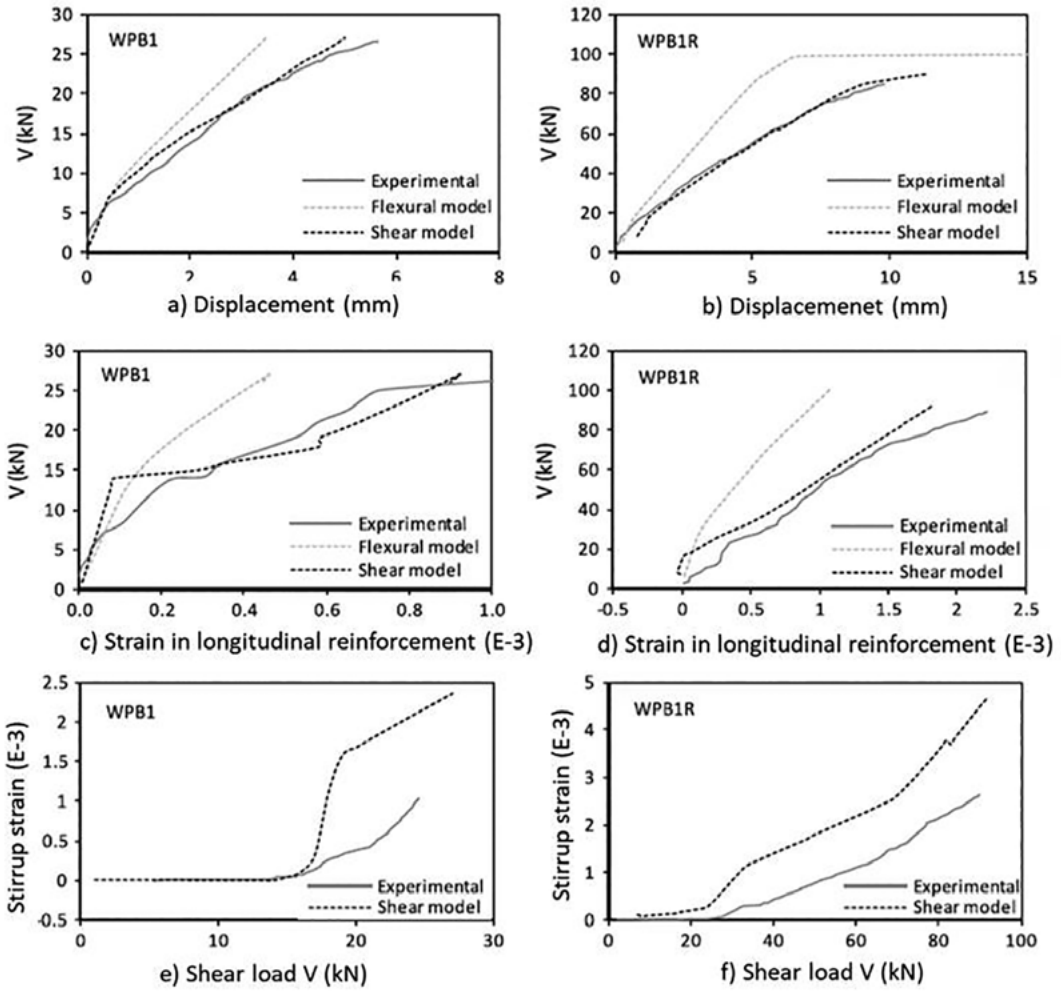

Figure 18. Comparison experimental and modelled response of the first damage test (WPB1) and the repaired structure up to failure (WPB1R). a, b) Force-displacement, c,d) strain in longitudinal (based on [17])

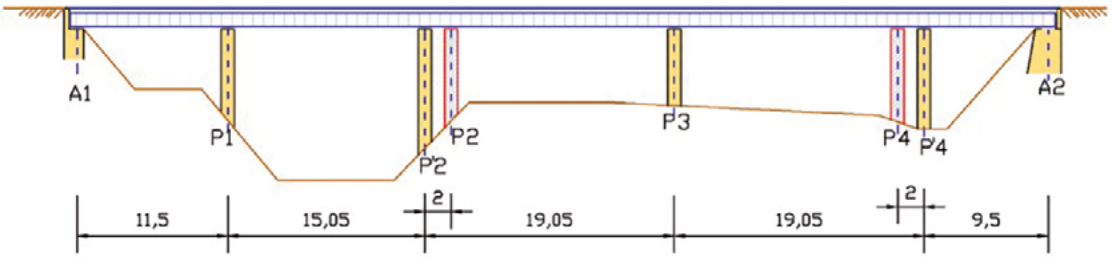

Figure 19. Front view of the bridge studied.

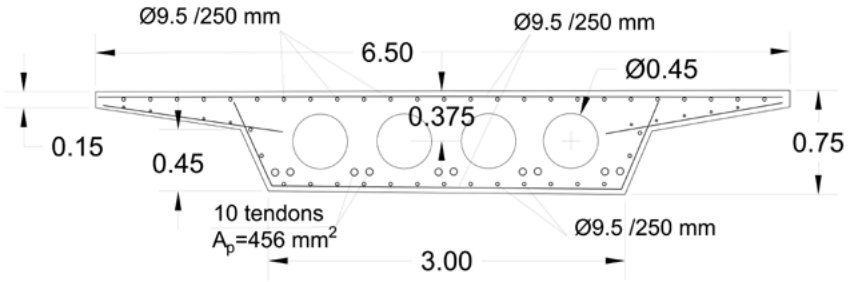

Figure 20. Cross-section and reinforcement at the bridge mid-span.

Figures 18d and 18e show the strain in the transversal reinforcement with the applied load for the initial load test and the repaired structure, respectively. The reported strains are located in the cross-section at 0.36 m from the support and 5.5 cm above the stirrup bottom-line. The numerical model correctly captures the initiation shear cracking and the activation of the transverse reinforcement. However, the model tends to over-predict the transversal strains. This difference can be explained due the use of the smeared crack approach in the constitutive model, as oppose to discrete cracking. Actual strains in the specimens shows abrupt variations, being larger in the points of the bar that coincide with the crack and smaller in between cracks. Conversely, in the smeared crack model, the strains distribution is smoother.

4. CASE STUDY: REMODELLING OF A POST-TENSIONED CONCRETE BRIDGE CROSSING THE AP-7 FREEWAY IN SPAIN

4.1. Definition of the problem and description of the analysed structure.

Due to the need of increasing the number of lanes of freeway AP-7 near Barcelona (Spain), the intermediate piers of several overcrossing bridges had to be moved 2m towards the abutments (Figure 19). In this paper, the developed analytical model has been used to simulate the strengthening operations carried out over one of the bridges affected by this remodelling, called OF29-3, in order to assess the serviceability and safety of the bridge during and after the intervention. In addition, the model has been used to analyse an alternative solution, based on external prestressing, proposed during the bidding process, to compare the efficiency of both solutions in terms of serviceability performance and safety. The design of the strengthening solution was carried out by Martinez Calzón [4].

The overcrossing consists of a 5 spans continuous post-tensioned concrete slab deck with constant depth, circular voids, and cap beams over the supports, see figure 20. The original span lengths were 11.5m + 3 × 17.05m + 11.5m (see figures 19 to 21). After the shifting of the internal piers P2 and P4, the span lengths became 11.5m + 15.05m + 21.05m + 21.05m + 9.5m. Concrete compressive characteristic strength was 35 MPa. The bridge was post-tensioned with 10 tendons of steel strength fpu=1700 MPa, providing a prestressing force of 582 kN per tendon (Api=456 mm^2). The tendon layout is the typical one of a continuous beam.

4.2. Description of the remodelling solution adopted

After building the two new piers, the bridge deck had to be uplifted from the old piers and supported on the new ones. The solution to be designed had to provide the concrete deck with the necessary strength and stiffness to resist the loads with the new span lengths, but also had to be built without interrupting the traffic. The solution adopted consisted of placing two longitudinal steel beams under the side cantilevers of the bridge deck, which were supported over the new piers. These beams were connected by means of transverse prestressing to the concrete deck (figure 21), over the old piers position. In this way, the support of the bridge deck did not change its position, although instead of being supported on the concrete pier, leaned on the longitudinal steel beams.

The transfer of the reactions from the old piers to the steel beam was made by means of hydraulic jacks which introduced an ascendant vertical load on the deck and at the same time a descendant vertical load on the steel beams. In this way the steel beams were deformed before they were connected to the deck and therefore had to be constructed with a pre-deformed shape.

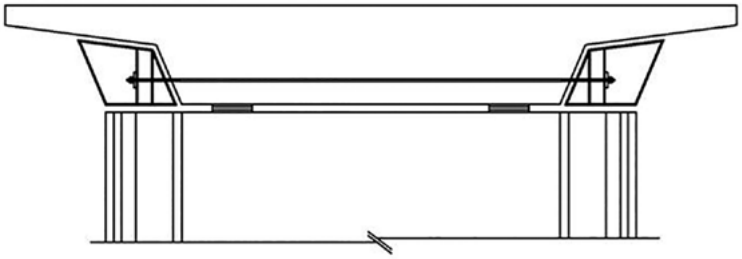

Figure 21. Strengthening solution adopted. Cross-section at the old piers position.

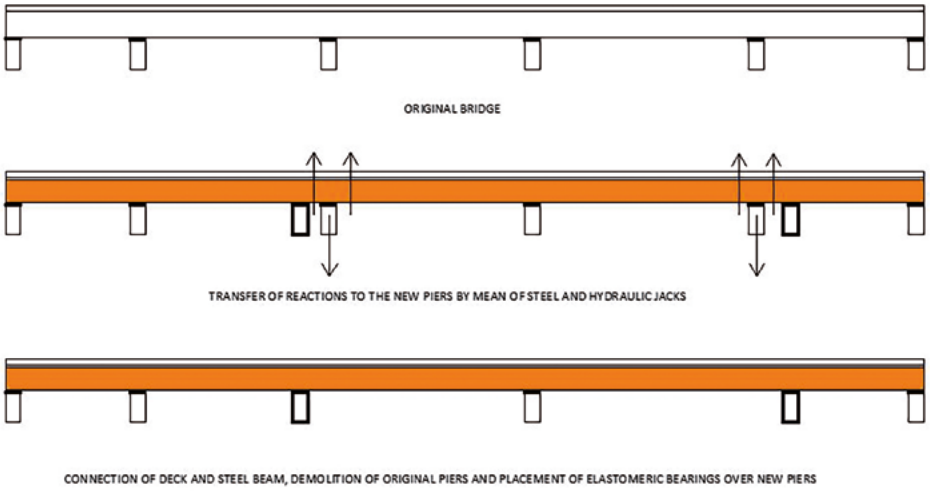

Figure 22. Strengthening operations: of transfer of reactions to steel beam and connection.

Figure 23. View of the strengthened bridge. Taken from Martínez Calzón [4].

By means of this system, the concrete deck did not suffer any change in stresses under permanent loads. Soft elastomeric bearings were placed over the new supports to compensate the effects of the beam flexibility on the bending moments due to live loads. A scheme of the procedure adopted for the reactions transfer and a view of the remodelled bridge can be seen in figure 22.

Figure 23 shows a picture of the strengthened bridge.

4.3. Numerical simulation of the strengthening process.

The bridge response was simulated starting from its construction. First, a time-dependent analysis to evaluate the long-term reactions to be transferred from piers P2 and P4 to the new piers was performed. Then, the steel beam was then placed on site subjected to its self-weight. The calculated reactions in piers P2 and P4 were introduced as two equal vertical external loads of opposite sense over those piers (downwards) and over the steel beam (upwards), simulating the loads introduced by the hydraulic jacks. Then, the beam supports representing piers P2 and P4 were eliminated, simulating the piers demolition. Table 4 shows the calendar of events affecting the structural response of the bridge along its service life, starting from the initiation of its construction, indicating the construction steps and the strengthening operations.

TABLE 4.
Calendar of events the studies bridge.

Step Nº	*Description of the construction step*	*Duration (days)*	*Age (days)*
1	Self-weight of the deck and transfer of prestressing	28	28
2	Pass of time until dead load is applied at 100 days	72	100
3	Application of dead load (16,3 kN/m)	0	100
4	Pass of time until initiation of remodelling at 7900 days	7900	8000
5	Placement of steel beam supported on the new piers PN2 and PN4	0	8000
6	Introduction of jack loads to uplift deck, supported on the steel beam	0	8000
7	Pass of time until connecting steel beam to deck operations	30	8030
8	Execution of connections between steel beam and slab at old supports	0	8030
9	Remove the jacks and the corresponding loads	0	8030
10	Place elastic supports on piers PN2 and PN4 and remove piers P2 and P4	0	8030

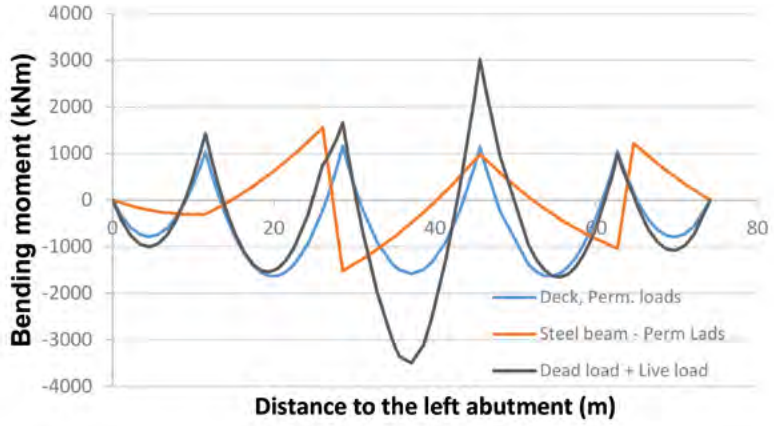

Figure 24. Bending moments law of remodelled bridge under live load on the whole bridge.

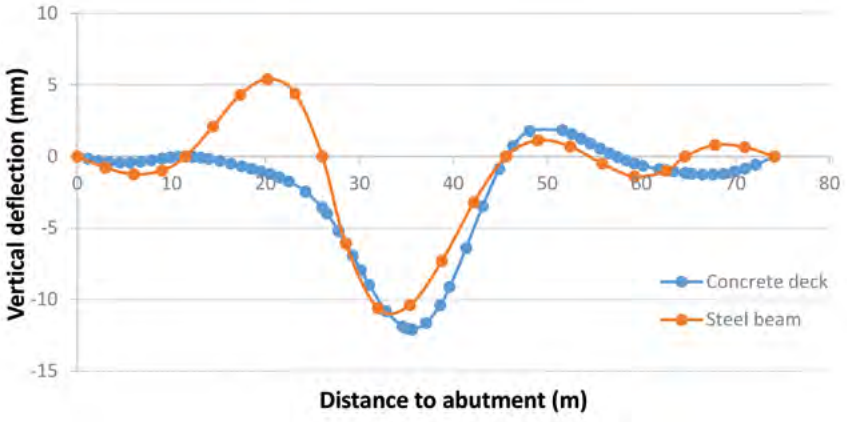

Figure 25. Deflection of the deck and steel beam under live load on the whole bridge length.

Figure 24 shows the bending moments law of remodelled bridge. The discontinuous line shows the moments law under the permanent loads, which coincides with that of the bridge before strengthening, because the only structural effects have been to substitute the reactions by the equal jack forces. However, the moments under the live load applied on the entire bridge length, have a reduction of the peak at pier 2, because of the flexibility of the steel beams that supports the concrete deck at the position of the old pier.

Figure 25 shows the displacements at the concrete deck and the steel beam, under the live loads. It is observed that both elements have the same deflection in the connecting point.

5.4. Evaluation of an alternative solution using external prestressing

An alternative strengthening solution based on external prestressing was analysed and their results compared with those

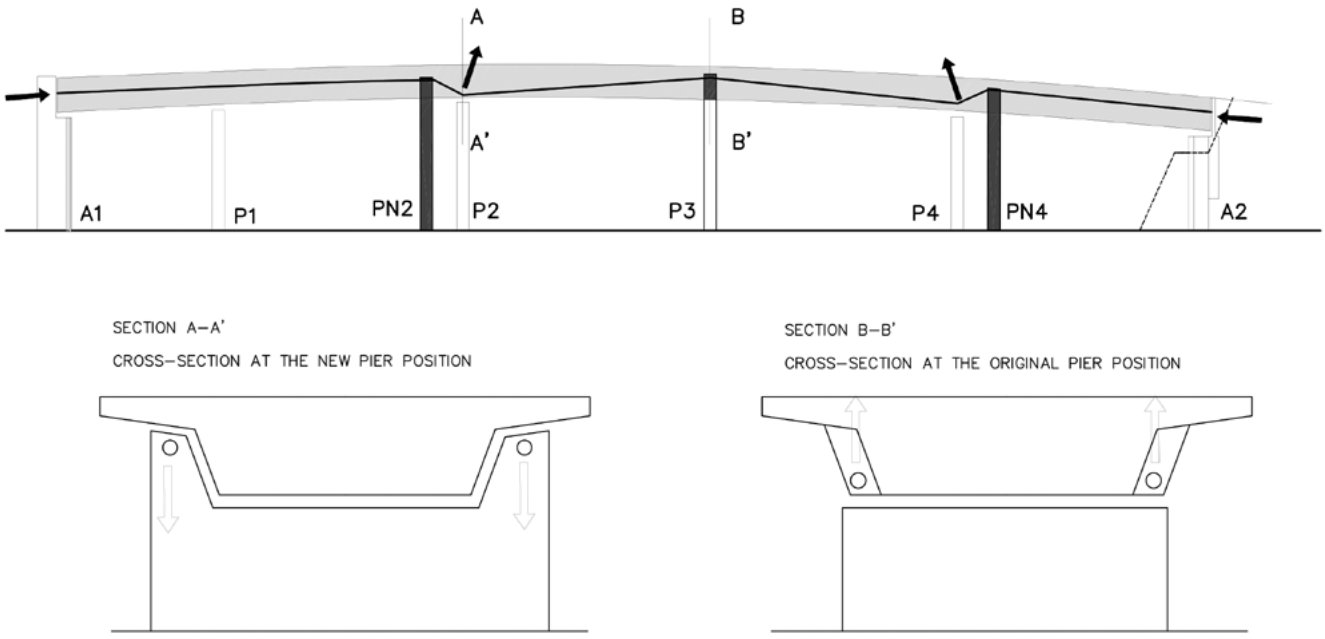

Figure 26. Strengthening system using external prestressing (solution 2).

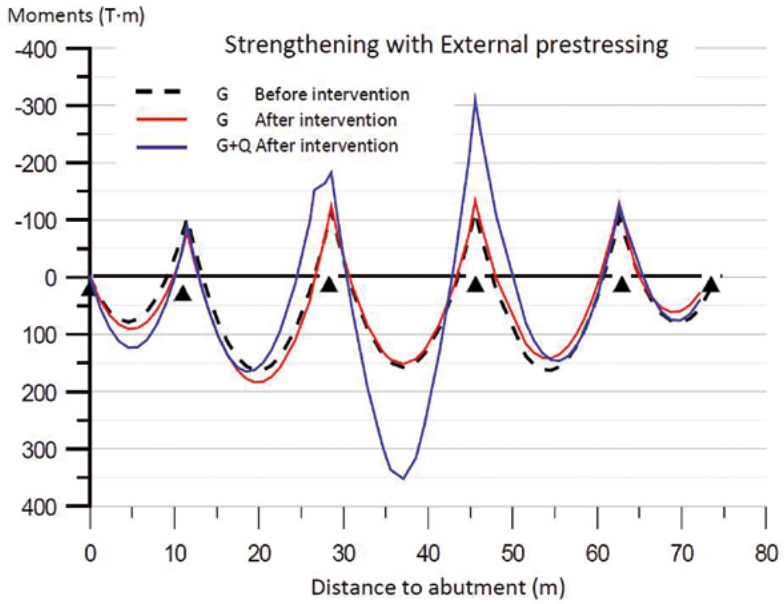

Figure 27. Bending moments in the original and strengthened deck with external prestressing.

of the actually built solution. It was proposed to place two longitudinal external prestressing tendons under the deck flanges, as shown in figure 26. The lower deviators of the external prestressing are anchored to the bridge deck over the original piers P2 and P4, while the upper deviators are anchored over piers PN2, P3 and PN4. Stressing the tendons produces an ascendant deviation load over piers P2 and P4 and descendant deviation loads over pier P3 and new piers PN2 and PN4, so that the reactions of piers P2 and P4 are automatically transferred to the new piers. The prestressing loads, obtained by equilibrium of forces, introduce an additional compressive stress in the deck which is favourable in front of cracking and flexure, shear and torsion strengths.

4.4. Results of the structural analysis

Bending moments under permanent loads before and after strengthening with external prestressing are shown in figure 27. It can be seen that the bending moments slightly changes with respect to those of the original bridge. The bending moments under the live load are quite similar to those estimated in the case of strengthening system 1.

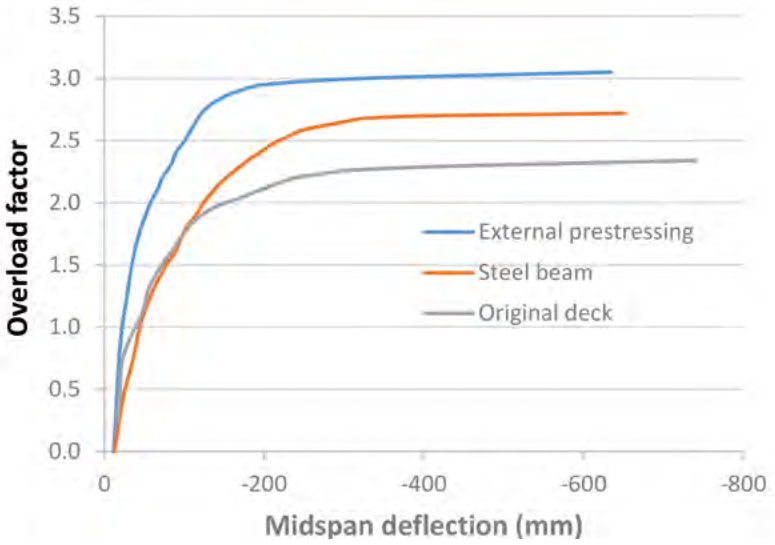

Figure 28. Load deflection curves.

In order to compare the performance of the structure in both cases, an incremental analysis up to failure was performed. Figure 28 shows the load-displacement curves of the bridge deck including the original bridge and the two strengthening solutions.

It can be seen that both solutions increase the stiffness and the strength of the structure. The solution using external prestressing provides a higher stiffness, especially in the post-cracking state, although under service load levels there are almost no differences. However, at ultimate load level, the external prestressing provides higher flexural strength than the use of a steel beam, because of the higher steel strength and the additional compression provided by the prestressing in a region of ductile flexural failure.

Nevertheless, due to lower cost, technical easiness and higher versatility of the system, solution 1 looks to be more adequate and was the one chosen.

5. CONCLUSIONS

An evolutionary analysis model capable to simulate, among others, the effects of phased construction processes, corrosion of steel or other materials deterioration processes and interventions for strengthening or remodelling, has been presented. In addition, the model can capture different types of failure, such as flexural and shear failures and can account for the effects of delamination in FRP strengthened structures using FRP laminates.

The model has been verified with the results of two tests on strengthened structures, one in flexure using FRP and the other in shear using enlargement of the section and additional shear reinforcement. In both cases, the model has shown its capacity to adequately simulate the behaviour of the strengthened structure.

In addition, two solutions for the remodelling of a freeway overcrossing in which two piers had to be shifted to widen the freeway roadway have been studied, and their efficiency compared. The model has shown to be capable to simulate all operations needed to carry out the required intervention. It has been shown that the actually constructed solution resulted to be very adequate to solve the structural problems faced with high versatility and constructive simplicity. On the other hand, the alternative solution, based on external prestressing, increases the un-cracked range and the flexural capacity of the deck, with less amount of materials. However, it is a more complex solution and not as versatile as the constructed one.

The combination of construction steps, time steps, load steps and equilibrium iterations to satisfy the effects of material non-linearity, allows considering the state of the structure along its entire service life. With respect to strengthening efficiency, the model allows evaluating the state of stresses, strains, and damage previous to the intervention, thus providing an accurate evaluation of the safety and serviceability performance of the remodelled structures than usual linear-elastic models.

Furthermore, the proposed model has shown to be a very useful tool to compare the efficiency and adequacy of different strengthening solutions, thus contributing to design safer, less expensive and more sustainable strengthening or remodelling interventions.

Acknowledgements

This paper is dedicated to the memory of an extraordinary engineer and human being, Luis Ortega Basagoiti, who was an example and reference for structural engineers and researchers along his professional career. The works described in this paper have been developed in the framework of the following research projects funded by the Spanish Science and Technology Ministries and by the European Funds for Regional Development, ADRESS (BIA2009-11764), REHABCAR (IPT-370000-2010-029), HORVITAL (BIA2015-64672-C4-1-R) and STRADURAVIUS (RTI2018-097314-B-C21).

References

[1] Macchi, G., Calvi, G.M., Sullivan, T.J., (2018) Structural Strengthening and Retrofit; Motivations, Concepts and Approaches, 1–24. https://doi.org/10.1007/978-981-10-5858-5_1.

[2] Aparicio García, J. (2019) Corte de soporte o pilar sin gatos. Postesado para estructura metálica: método cuña-contracuña; tecnología derivada., *Hormigón y Acero*. 70(288) 35–55. https://doi.org/10.33586/hya.2019.002.

[3] Priestley, M., Seible, F., Calvi, M. (1996) Seismic design and retrofit of bridges.

[4] Martínez Calzon, J., (1995) Ampliación de las luces de 15 pasos superiores continuos postensados, para conseguir el ensanchamiento a seis carriles de la autopista AP-7 Barcelona-La Junquera, Tramo: Hostalric-Maçanet, *Hormigón y Acero* 46(196) 133–146.

[5] Astiz, M.A., Ortega Basagoiti, L., Floriano, M. (2005) Reducción de vibraciones por efecto del viento en la torre de control de un aeropuerto, in: II Congr. Puentes y Estructuras Edif. ACHE , Zaragoza.

[6] Khaled, H., Nabil, A., Nageh, M., Magdy, T. (2014) State-of-the Art Review: Strengthening of Reinforced Concrete Structures – Different Strengthening Techniques, in: *Sixth Int. Conf. NANO-TECHNOLOGY Constr.* (NTC 2014), Cairo.

[7] Trinh, J.L. (1987) Structural Strengthening by External Prestressing, in: S.N. and E. Absi (Ed.), *Bridg. Eval. Repair Rehabil.*, The University of Michigan, Ann Arbor, MI.

[8] Hollaway, L. (1999) Strengthening of Reinforced Concrete Structures. Using externally bonded FRP composites in *Structural and Civil Engineering*, Woodhead P.

[9] fib (2019) Externally applied FRP reinforcement for concrete structures, fib bulletin 90.

[10] ACI Committee 562 (2012), ACI Requirements for Evaluation, Repair and Rehabilitation of Concrete Buildings (ACI 652-13) and Commentaries.

[11] Calderón Bello, E., Díaz-Pavón Cuaresma, E. (2018) Dificultades en el planteamiento del refuerzo de pilares de hormigón armado, *Hormigón y Acero*. 69 (284) 49–58. https://doi.org/10.1016/j.hya.2017.09.001.

[12] Kang, Y.J., Scordelis, A.C. (1990) Non-linear segmental analysis of reinforced and prestressed concrete bridges., in: *3rd Int. Conf. Short Mediu. Spam Bridg.*: pp. 229–240.

[13] Marí, A.R. (2000) Numerical simulation of the segmental construction of three dimensional concrete frames, *Eng. Struct.* 22, 585–596. https://doi.org/10.1016/S0141-0296(99)00009-7.

[14] Marí, A. (1984) *Nonlinear Geometric, Material and Time-dependent Analysis of Three Dimensional Reinforced and Prestressed Concrete Frames*, UCB /SESM, University of California, Berkeley.

[15] Mari, A., Bairan, J.M., Moreno, R., Oller, E., Alvarez, J. (2012) Numerical simulation of bridges remodeling, in: *Int. Conf. Bridg. Maintenance, Saf. Manag.*: pp. 2032–2039.

[16] Ferreira, D., Bairán, J., Marí, A. (2015) Efficient 1D model for blind assessment of existing bridges: simulation of a full-scale loading test and comparison with higher order continuum models, Struct. Infrastruct. Eng. 11, 1383–1397. https://doi.org/10.1080/15732479.2014.964734.

[17] Ferreira, D., Bairán, J., Marí, A. (2013) Numerical simulation of shear-strengthened RC beams, *Eng. Struct.* 46, 359–374. https://doi.org/10.1016/j.engstruct.2012.06.050.

[18] Ferreira, D., Oller, E., Marí, A., Bairán, J. (2013) Numerical Analysis of Shear Critical RC Beams Strengthened in *Shear with FRP Sheets, J. Compos. Constr.* 17, 04013016. https://doi.org/10.1061/(asce)cc.1943-5614.0000434.

[19] Ferreira, D., Oller, E., Marí, A., Bairán, J. (2016) Analysis of FRP Shear Strengthening Solutions for Reinforced Concrete Beams Considering Debonding Failure, *J. Compos. Constr.* 20 04016018. https://doi.org/10.1061/(asce)cc.1943-5614.0000672.

[20] Oller, E. Ferreira, D., Marí, A., Bairán, J.M. (2018) Numerical analysis of reinforced concrete beams strengthened in shear by externally bonded (EB) fibre reinforced polymer (FRP) sheets, *Hormigón y Acero*. 69(285) 113–120. https://doi.org/10.1016/j.hya.2017.04.022.

[21] Bairan, J.M., Fernandez, I., Moreno, R., Mari, A., Velázquez, C. (2014) Efectos de la corrosión de las armaduras en su curva tensión-deformación y resistencia a fatiga. Modelo y calibración experimental, in: *Congr. La Asoc. Científico-Técnica Del Hormigón Estructural*: pp. 91–92.

[22] Oller, E., Cobo, D., Marí, A.R. (2009) Interface Behavior in Fiber-Reinforced Polymer-Strengthened Beams Subjected to Transverse Loads: Maximum Transferred Force, *J. Compos. Constr.* 13, 35–44. https://doi.org/10.1061/(asce)1090-0268(2009)13:1(35).

[23] Teng, J.G., Smith, S.T., Yao, J., Chen, J.F. (2003) Intermediate crack-induced debonding in *RC beams and slabs, Constr. Build. Mater.* 17, 447–462. https://doi.org/10.1016/S0950-0618(03)00043-6.

[24] Ye, L.P., Lu, X.Z., Chen, J.F. (2005) Design proposals for debonding strengths of FRP strengthened RC beams in the Chinese Design Code, in: *Proc., Int. Symp. Bond Behav. FRP Struct. Int. Inst. FRP Constr.* (IIFC), Hong Kong, China.

[25] Chen, J.F., Yuan, H., Teng, J.G. (2007) Debonding failure along a softening FRP-to-concrete interface between two adjacent cracks in concrete members, *Eng. Struct.* 29 259–270. https://doi.org/10.1016/j.engstruct.2006.04.017.

[26] Lu, X.Z., Teng, J.G., Ye, L.P., Jiang, J.J. (2007) Intermediate Crack Debonding in FRP-Strengthened RC Beams: FE Analysis and Strength Model, *J. Compos. Constr.* 11 161–174. https://doi.org/10.1061/(asce)1090-0268,11:2(161).

[27] Wu, Z., Niu, H. (2007) Prediction of Crack-Induced Debonding Failure in R/C Structures Flexurally Strengthened With Externally Bonded Frp Composites, *Doboku Gakkai Ronbunshuu E.* 63, 620–639. https://doi.org/10.2208/jsceje.63.620.

[28] Said, H., Wu, Z. (2008) Evaluating and proposing models of predicting IC debonding failure, *J. Compos. Constr.* 12284–299.

[29] Faella, C., Martinelli, E., Nigro, E. (2008) Formulation and validation of a theoretical model for intermediate debonding in *FRP-strengthened RC beams, Compos. Part B Eng.* 39, 645–655. https://doi.org/10.1016/j.compositesb.2007.06.002.

[30] Matthys, S., (2000) *Structural behaviour and design of concrete members strengthened with externally bonded FRP reinforcement*, University of Ghent, Belgium.

[31] D'Antino, T., Triantafillou, T.C. (2016) Accuracy of design-oriented formulations for evaluating the flexural and shear capacities of *FRP-strengthened RC beams, Struct. Concr.* 17, 425–442. https://doi.org/10.1002/suco.201500066.

[32] Oller, E., Marí, A.R., Bellido, L. (2013) Design method for flexural strengthening with fiber reinforced polymer (FRP) laminates avoiding its premature debonding, *Inf. La Construcción*. 65 519–531. https://doi.org/10.3989/ic.12.087.

[33] Ferreira, D., Marí, A., Bairán, (2014) J. Assessment of prestressed concrete bridge girders with low shear reinforcement by means of a non-linear filament frame model, *Struct. Infrastruct. Eng.* 10, 1531–1546. https://doi.org/10.1080/15732479.2013.834944.

[34] Ferreira, D., Bairán, J., Marí, A., Faria, R. (2014) Nonlinear analysis of RC beams using a hybrid shear-flexural fibre beam model, *Eng. Comput.* (Swansea, Wales). 31, 1444–1483. https://doi.org/10.1108/EC-04-2013-0114.

[35] Ferreira, D., Bairán, J.M., Marí, A. (2017) Influence of time-dependent restrained strains in the shear response of RC frames, *Mater. Struct. Constr.* 50. https://doi.org/10.1617/s11527-016-0875-8.

[36] Bairan, J.M., Marí, A.R. (2006) Coupled model for the non-linear analysis of anisotropic sections subjected to general 3D loading. Part 1: Theoretical formulation, *Comput. Struct.* 84 2254–2263. https://doi.org/10.1016/j.compstruc.2006.08.036.

[37] Bairan, J.M., Mari, A.R. (2007) Multiaxial-coupled analysis of RC cross-sections subjected to combined forces, *Eng. Struct.* 29 1722–1738. https://doi.org/10.1016/j.engstruct.2006.09.007.

[38] Ceresa, P., Petrini, L., Pinho, R., Sousa, R. (2009) A fibre flexure-shear model for seismic analysis of RC-framed structures, Earthq. *Eng. Struct. Dyn.* 38, 565–586. https://doi.org/10.1002/eqe.894.

[39] Navarro Gregori, J., Miguel Sosa, P., Fernández Prada,M.A., Filippou, F.C. (2007) A 3D numerical model for reinforced and prestressed concrete elements subjected to combined axial, bending, shear and torsion loading, *Eng. Struct.* 293404–3419. https://doi.org/10.1016/j.engstruct.2007.09.001.

[40] Mohr, S., Bairán, J.M., Marí, A.R. (2010) A frame element model for the analysis of reinforced concrete structures under shear and bending, *Eng. Struct.* 32 3936–3954. https://doi.org/10.1016/j.engstruct.2010.09.005.

[41] Le Corvec, V. (2012) Nonlinear 3d frame element with multi-axial coupling under consideration of local effect.

[42] Di Re, P. (2017) *3D beam-column finite element under tri-axial stress-strain states: non-linear shear stress distribution and warping*, Univeristy La Sapienza.

[43] Kagermanov, A., Ceresa, P. (2017) Fiber-Section Model with an Exact Shear Strain Profile for Two-Dimensional RC Frame Structures, *J. Struct. Eng.* 143, 04017132. https://doi.org/10.1061/(asce)st.1943-541x.0001839.

[44] Poliotti, M., Bairán, J.M. (2020) B-spline sectional model for general 3D effects in reinforced concrete elements, *Eng. Struct*. 207. https://doi.org/10.1016/j.engstruct.2020.110200.

[45] Bairan, J.M., Mari, A.R. (2007) Shear-bending-torsion interaction in structural concrete members: A nonlinear coupled sectional approach, *Arch. Comput. Methods Eng.* 14 249–278. https://doi.org/10.1007/s11831-007-9007-5.

[46] Cladera, A., Marí, A., Ribas, C., Bairán, J., Oller, E. (2015) Predicting the shear-flexural strength of slender reinforced concrete T and I shaped beams, *Eng. Struct*. in review. https://doi.org/10.1016/j.engstruct.2015.07.025.

[47] Mari, A.R., Bairán, J.M,. Cladera, A., Oller, E., Ribas, C. (2014) Shear-flexural mechanical model for the design and assessment of reinforced concrete beams, *Struct. Infrastruct. Eng.* doi: 10.1080/15732479.2014.964735. https://doi.org/10.1080/15732479.2014.964735.

[48] Celada, U., Bairan, J.M., Mari, A., Pujol, M., Oller, E. (2014) Sobre el cortante en secciones en T y sus mecanismos resistentes, in: *Congr. La Asoc. Científico-Técnica Del Hormigón Estructural*: pp. 205–206.

[49] El-Refaie, S.A., Ashour, A.F., Garrity, S.W. (2003) CFRP strengthened continuous concrete beams, *Proc. Inst. Civ. Eng. Struct. Build.* 156, 395–404. https://doi.org/10.1680/stbu.2003.156.4.395.

[50] (CEN) European Committee for Standardization (2016) Eurocode 2: Design of concrete structures. Part 1-1: General rules and rules for buildings, Eur. Com. Stand. https://doi.org/[Authority: The European Union Per Regulation 305/2011, Directive 98/34/EC, Directive 2004/18/EC].

[51] Comisión Permanente del Hormigón (2008) Instrucción del hormigón estructural EHE-08.

[52] Marí, A.R., Oller, E., Bairán, J.M. (2011) Predicting the Response of FRP-Strengthened Reinforced-Concrete Flexural Members with Nonlinear Evolutive Analysis Models, *J. Compos. Constr.* 15 (2011) 799–809. https://doi.org/10.1061/(asce)cc.1943-5614.0000214.

[53] Souza, R.H.F., Appleton, J. (1997) Behaviour of shear-strengthened reinforced concrete beams, *Mater. Struct. Constr.* 30, 81–86. https://doi.org/10.1007/bf02486308.